Available online at www.sciencedirect.com
SCIENCE DIRECT
International Journal of Heat and Fluid Flow 27 (2006) 476–489
International Journal of HEAT AND FLUID FLOW
www.elsevier.com/locate/ijhff

Turbulent natural convection in an air-filled isosceles triangular enclosure

El Hassan Ridouane [a,*], Antonio Campo [b], Mohammed Hasnaoui [a]

[a] LMFE, Department of Physics, Faculty of Sciences Semlalia, B.P. 2390, Marrakech, Morocco
[b] Department of Mechanical Engineering, The University of Vermont, Burlington, VT 05405, USA

Received 12 February 2005; accepted 15 October 2005
Available online 10 January 2006

Abstract

This paper addresses turbulent natural convection of air confined in an isosceles triangular enclosure representing conventional attic spaces of houses and buildings with pitched roofs and horizontally suspended ceilings. The values to be considered are $H = 0.86$ m and 2.73 m for the height while the values 1.72 m and 5.46 m were assigned to the width, W, such as the aspect ratio H/W remains 0.5. The third dimension of the cavity is considered long enough for the flow to be considered 2D. The base wall is heated at 20 °C and the inclined walls are cooled at 0 °C. This combination of factors leads to large Rayleigh numbers equal to 1.58×10^9 and 5×10^{10}. Turbulence is modeled by a low-Reynolds-number k–ε model. The system of governing equations, subject to the proper boundary conditions is solved with the finite volume method. Second-order-accurate QUICK and SIMPLE schemes were used for the discretization of the convective terms and the pressure–velocity coupling, respectively. The velocity and temperature distributions were calculated at different locations in the cavity and their mean quantities are presented. The local and average Nusselt numbers and the wall shear stresses are also presented. Since to the knowledge of the authors, no previous results on turbulent thermal convection in this geometry exist, the validation of the numerical code was performed by comparing velocity and temperature profiles against recent experimental measurements, obtained for a square cavity. Satisfactory agreement was observed.

Keywords: Isosceles triangular enclosure; Natural convection; k-ε turbulence model; Velocity distribution; Temperature distribution; Wall shear stress; Heat transfer

1. Introduction

Natural convection in enclosures has been extensively studied both numerically and experimentally. In the area of numerical studies, natural convection in enclosures represents one of the simplest multiple-scale, coupled non-linear fluid flow problems that provide a convenient vehicle for the development of new analyses and new numerical algorithms. Among the various types of enclosures, the triangular enclosure was extensively studied because many engineering systems can be accommodated into this configuration. Typical examples include attics of houses and buildings, electronic equipment and others. The first works devoted to the isosceles triangular geometry were concentrated on laminar flows and the majority of them were completed with considerable success. In this kind of enclosed space, two different scenarios are possible depending on the season of the year. In the wintertime, the attic is heated at the base and symmetrically cooled at the inclined walls, whereas in the summertime, the attic is cooled at the base and symmetrically heated at the inclined walls.

The literature review concerning natural convection in isosceles triangular cavity shows that this configuration was the object of experimental and numerous numerical studies. Earlier, the flow and temperature patterns, local wall heat fluxes and mean heat flux rates were measured experimentally by Flack (1979, 1980) in isosceles triangular cavities with three different aspect ratios. The cavities, filled

* Corresponding author. Tel.: +1 802 656 0978; fax: +1 802 656 1929.
E-mail address: eridouan@cems.uvm.edu (E.H. Ridouane).

0142-727X/$ - see front matter © 2005 Elsevier Inc. All rights reserved.
doi:10.1016/j.ijheatfluidflow.2005.10.013

Nomenclature

A_W	aspect ratio, $A_W = H/W$
c_p	specific isobaric heat capacity (J/kg K)
C_μ, $C_{1\varepsilon}$, $C_{2\varepsilon}$	empirical constants
f_μ, f_1, f_2	wall-damping functions
g	acceleration due to gravity (m/s^2)
h	local convective heat transfer coefficient (W/m^2 K)
$\overline{h}$	mean convective heat transfer coefficient (W/m^2 K)
H	enclosure height (m)
k	turbulent kinetic energy (m^2/s^2)
L	inclined wall length (m)
Nu	local Nusselt number, Eqs. (11a) and (11b)
$\overline{Nu}$	mean Nusselt number, $\overline{Nu} = \int_0^1 Nu\,\mathrm{d}\eta$
p	static pressure (Pa)
Pr	Prandtl number, $Pr = \upsilon/\alpha$
Pr_T	turbulent Prandtl number, $Pr_T = \upsilon_T/\alpha_T$
Ra_H	Rayleigh number, $Ra_H = g\beta(T_H - T_C)H^3/\alpha\upsilon$
Re_T	turbulence Reynolds number, $Re_T = k^2/\upsilon\varepsilon$
T	temperature (K)
T_C	cold wall temperature (K)
T_H	hot wall temperature (K)
T_r	reference temperature, $T_r = (T_H + T_C)/2$ (K)
u, v	velocities in the x- and y-directions (m/s)
U, V	time-averaged velocities in the x- and y-directions (m/s)
W	enclosure base (m)
x, y	horizontal and vertical coordinates (m)
X	dimensionless horizontal coordinate, $X = x/W$
z_1, z_2	coordinate along the left and right inclined walls (m)
Z_1, Z_2	dimensionless coordinate along the left and right inclined walls, $Z_i = z_i/L$

Greek letters

α	thermal diffusivity, $\alpha = \lambda/\rho c_p$ (m^2/s)
β	coefficient of volumetric thermal expansion (1/K)
ε	turbulent eddy dissipation
λ	thermal conductivity (W/m K)
η	refers to X, Z_1, and Z_2 when integrating along the base, left, and right inclined walls, respectively
μ	molecular dynamic viscosity (kg/m s)
μ_T	turbulent viscosity (kg/m s)
υ	molecular kinematic viscosity (m^2/s)
θ	dimensionless temperature, $(T - T_C)/(T_H - T_C)$
ρ	fluid density (kg/m^3)
σ_k, σ_ε	turbulent Schmidt numbers
τ_w	wall shear stress (Pa)

Superscript

$'$	fluctuation component

with air, were heated/cooled from the base and cooled/heated from the inclined walls covering a wide range of Grashof numbers. Akinsete and Coleman (1982) conducted a numerical study based on the finite-difference method on natural convection flow of air contained in a right-triangular cavity (half of the isosceles triangular cavity) with a cold base, heated inclined wall and insulated vertical wall. Numerical solutions were obtained for height-base ratios $\leqslant 0.5$ in conjunction with Grashof numbers varying up to a maximum value of 8000. Poulikakos and Bejan (1983) reported a theoretical and numerical investigation of natural convection inside a right-triangular cavity with cold inclined wall, warm base and insulated vertical wall. The theoretical fluid flow and temperature fields were determined on the basis of an asymptotic analysis valid for shallow spaces with aspect ratios approaching zero. Another phase of the study focused on the temporal evolution of the velocity and temperature fields using various aspect ratios of the cavity.

Using vorticity-stream function formulation, and a numerical method based on the finite-element method, Del Campo et al. (1988) examined natural convection in the entire isosceles triangular cavities for several combinations of thermal boundary conditions applied on their walls. For the particular case of heating from below and cooling from above, the computed velocity and temperature fields obtained at low Grashof numbers, were found to be symmetrical with respect to the mid-plane of symmetry in a cavity having aspect ratio of unity. Salmun (1995) studied a two-dimensional convection problem in a right-triangular cavity filled with air or water for various aspect ratios and Rayleigh numbers. The governing equations, written in transient form, were solved numerically and the obtained results were confirmed using two independent methods. The numerical experiments conducted showed that the single-cell circulation is not stable in the parametric domain considered. This solution breaks down as the Rayleigh number is increased beyond $3 \times 10^3$and a new steady-state is achieved, that of a multi-cellular type. Asan and Namli (2000) conducted a numerical study of laminar natural convection in a pitched roof of triangular cross-section considering an adiabatic mid-plane wall condition in their numerical procedure. Only summertime conditions were considered over wide ranges of both the Rayleigh number and the height-based aspect ratio. Their results showed that most of the heat exchange takes place near the intersection of the active walls.

The finite-element method was used by Holtzman et al. (2000) to model the complete isosceles triangular cavity without claiming cavity symmetry. A heated base and

symmetrically cooled inclined walls were considered as thermal boundary conditions for various aspect ratios and Grashof numbers. These authors performed a flow visualization study to validate experimentally the existence of symmetry-breaking bifurcations in one cavity of fixed aspect ratio. This anomalous bifurcation phenomenon was intensified by gradually increasing the Grashof number. The main conclusion drawn in this paper was that, for identical isosceles triangular cavities engaging symmetrical and non-symmetrical assumptions, the differences in terms of mean Nusselt number were about 5%. It is worth adding that the majority of works cited above have assumed the existence of a vertical plane of symmetry passing through the middle of the isosceles triangular cavity in order to deal with a manageable computational domain that is half the size of the physical domain. Two years later, assuming a symmetrical nature of the flow within an attic space, Haese and Teubner (2002) investigated the thermal effects in building attics involving ceiling fans. The problem was solved for the winter conditions using the vorticity-stream function formulation. Recently, Ridouane and Campo (2005) generated experimental-based correlations for the reliable characterization of the center plane temperature and the mean convective coefficient in isosceles triangular cavities filled with air. The experimental data was gathered from various sources for various aspect ratios and Grashof numbers.

The heat transfer benefits derivable from connecting the bottom and top walls of attic enclosures with insulated vertical sidewalls, were investigated numerically by Ridouane et al. (in press). Different heights of the insulated sidewalls were chosen varying from a limiting isosceles triangle cavity to a limiting rectangle cavity. The Prandtl number was set at 0.71 (air as working fluid), and values of the Rayleigh number varying in the range $[10^3, 10^6]$ were assigned. The presence of insulated walls, even with a very small height, provides a huge gain of energy (for cooling in the summer or heating in the winter). On a related topic, Iyican et al. (1980a,b) studied analytically and experimentally natural convection in an inclined trapezoidal cavity heated from below and cooled from above. The cavity is formed with curved and parallel active walls and plane adiabatic sidewalls. The effect of tilt angle between the adiabatic walls ranging from 0° to 90° was investigated. Experimental data exhibited a minimum in the local Nusselt number curve between 90° and 0°. The angle where the minimum occurs is a function of the Rayleigh number and moves towards 90° as *Ra* increases. Comparison of the data with the results obtained with a two-dimensional theoretical analysis showed good agreement at 90°, but the agreement progressively deteriorated as the angle is decreased towards 45°. The authors proposed also correlation equations of the local Nusselt number for a wide range of *Ra*. Lam et al. (1989) investigated numerically and experimentally natural convection in a trapezoidal cavity composed of two vertical adiabatic sidewalls, a horizontal hot bottom wall, and an inclined cold top. Results were presented for a cavity with aspect ratio of 4, Rayleigh numbers varying in the range 10^3–10^7, and top surface inclinations sweeping from 0° to 25°. The results obtained illustrated that the onset of natural convection in a trapezoidal cavity occurs progressively at lower *Ra* as the angle of inclination was increased from 0°. The experimental heat transfer results were in good agreement with those computed numerically and indicated that the Nusselt number decreases with increment of the inclination angle. Numerical results concerning natural convection in trapezoidal enclosures with insulated horizontal bottom and top walls and inclined active sidewalls, were presented by Lee (1991) and Peric (1993) for Rayleigh numbers varying up to 10^5. Moukalled and Acharya (1997) and Moukalled and Acharya (2000) studied numerically natural convection heat transfer in partially divided trapezoidal cavities with partial dividers attached to the lower horizontal base (Moukalled and Acharya, 1997) or upper inclined surface (Moukalled and Acharya, 2000) of the cavity. For both cases considered, the presence of the baffles resulted in a relative decrease of heat transfer across the cavity up to 70%.

This paper addresses turbulent natural convection of air confined to an isosceles triangular cavity representing conventional attic spaces of houses and buildings with pitched roofs and horizontal suspended ceilings. When the top of an isosceles triangular cavity is symmetrically heated and the bottom wall is cooled (the situation encountered during the summer time), the velocity and temperature patterns are always stable regardless of the value of the Rayleigh number and the flow remains always laminar (Flack, 1979, 1980). The present study investigates the wintertime situation when the base is heated and the two inclined walls are symmetrically cooled. It was demonstrated by Flack (1980) that the flow becomes unsteady when the Rayleigh number exceeds a critical value of 6.25×10^5 for a cavity with an aspect ratio H/W of 0.5. This is the situation considered in the present study. Turbulence is modeled by a low-Reynolds-number k–ε model. The system of governing equations, subject to the proper boundary conditions is solved with the finite volume method. This approach takes into account the second-order-accurate QUICK and SIMPLE schemes for the discretization of the convective terms and the pressure–velocity coupling, respectively. Despite significant developments in the measurement techniques and instrumentation, as well as in the numerical methods with improved computing capacity, the study of turbulent natural convection in triangular geometries has not been reported yet. The objective of this paper is to fill this gap by performing numerical simulations of the turbulent airflow in an isosceles triangular cavity.

2. Formulation of the problem

Consider a two-dimensional isosceles triangular cavity of width W and height H filled with air as depicted in Fig. 1. The enclosure has two cold inclined walls at uniform temperature T_C and a hot base wall at uniform temperature

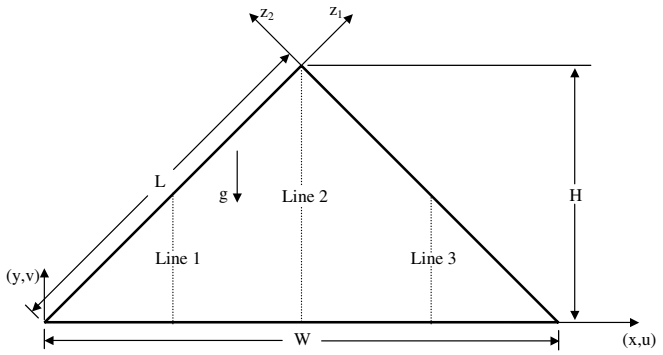

Fig. 1. Schematic of an air-filled isosceles triangular cavity.

T_H. The fluid properties appearing in Pr and Ra_H are evaluated at the reference temperature T_r. Owing that the study is aimed at natural convection in turbulent regime, the values 1.58×10^9 and 5×10^{10} were chosen for the Rayleigh number which correspond to a cavity exposed to a temperature difference $T_H - T_C = 20$ K with 0.86 m and 2.73 m height, respectively. In practical flows the mean density may vary and the instantaneous density always exhibits turbulent fluctuations (Versteeg and Malalasekera, 1995). Bradshaw et al. (1981) stated that small density fluctuations do not appear to affect the flow significantly. In free turbulent flows the velocity fluctuations can easily reach values around 20% of the mean velocity (Gutmark and Wygnanski, 1976; Champagne et al., 1976; Wygnanski et al., 1986). In such circumstances, the density fluctuations begin to affect the turbulent motion. To investigate the effects of the pertinent fluctuations the authors replace the flow variables **u** (velocity vector) and pressure p by the sum of a mean and fluctuating component. Thus

$$u = U + u';\quad v = V + v';\quad p = P + p'$$

The mathematical formulation for compressible buoyant flow is summarized as follows (Versteeg and Malalasekera, 1995):

$$\mathrm{div}(\rho\mathbf{U}) = 0 \tag{1}$$

$$\mathrm{div}(\rho U\mathbf{U}) = -\frac{\partial P}{\partial x} + \mathrm{div}[(\mu+\mu_T)\mathrm{grad}\,U] + \left[-\frac{\partial(\rho\overline{u'^2})}{\partial x} - \frac{\partial(\rho\overline{u'v'})}{\partial y}\right] \tag{2}$$

$$\mathrm{div}(\rho V\mathbf{U}) = -\frac{\partial P}{\partial y} + \mathrm{div}[(\mu+\mu_T)\mathrm{grad}\,V] + \left[-\frac{\partial(\rho\overline{u'v'})}{\partial x} - \frac{\partial(\rho\overline{v'^2})}{\partial y}\right] - \rho g \tag{3}$$

$$\mathrm{div}(\rho T\mathbf{U}) = \mathrm{div}\left[\left(\frac{\lambda}{c_P} + \frac{\mu_T}{Pr_T}\right)\mathrm{grad}\,T\right] \tag{4}$$

$$\mathrm{div}(\rho k\mathbf{U}) = \mathrm{div}\left[\left(\mu + \frac{\mu_T}{\sigma_k}\right)\mathrm{grad}\,k\right] + 2\mu_T E_{ij}\cdot E_{ij} - \rho\varepsilon \tag{5}$$

$$\mathrm{div}(\rho\varepsilon\mathbf{U}) = \mathrm{div}\left[\left(\mu + \frac{\mu_T}{\sigma_\varepsilon}\right)\mathrm{grad}\,\varepsilon\right] + C_{1\varepsilon}f_1\frac{\varepsilon}{k}2\mu_T E_{ij}\cdot E_{ij} - C_{2\varepsilon}f_2\rho\frac{\varepsilon^2}{k} \tag{6}$$

where the symbol ρ stands for the mean fluid density.

The fluid thermal conductivity is designated by λ to avoid confusion with k, which represents the turbulent kinetic energy. The eddy viscosity is obtained from k and ε by the Prandtl–Kolmogorov relation,

$$\mu_T = C_\mu f_\mu \rho\frac{k^2}{\varepsilon} \tag{7}$$

The preceding equations contain adjustable constants C_μ, σ_k, σ_ε, $C_{1\varepsilon}$ and $C_{2\varepsilon}$ that are chosen as 0.09, 1, 1.3, 1.44 and 1.92, respectively (Versteeg and Malalasekera, 1995). The constants C_μ, $C_{1\varepsilon}$ and $C_{2\varepsilon}$ are multiplied by wall-damping functions, f_μ, f_1 and f_2, respectively, that are themselves functions of the turbulence Reynolds number $Re_T = \frac{k^2}{\varepsilon v}$ and similar parameters. Further,

$$f_\mu = \left[1 - \exp\left(-0.0165Re_y\right)\right]^2\left(1 + \frac{20.5}{Re_T}\right) \tag{8}$$

$$f_1 = \left(1 + \frac{0.05}{f_\mu}\right)^3;\quad f_2 = 1 - \exp\left(-Re_T^2\right) \tag{9}$$

In the function f_μ the parameter Re_y is defined by $k^{1/2}y/v$ (Lam and Bremhorst, 1981). In addition, the symbol E_{ij} in Eqs. (5) and (6) denotes the rate of deformation of a fluid element in a turbulent flow given by

$$E_{xx} = \frac{\partial U}{\partial x};\quad E_{yy} = \frac{\partial V}{\partial y};\quad E_{xy} = E_{yx} = \frac{1}{2}\left[\frac{\partial U}{\partial y} + \frac{\partial V}{\partial x}\right] \tag{10}$$

3. Boundary conditions

The entire physical domain is taken into consideration for the computations and no symmetry plane is assumed. This step is necessary for the present problem because, as demonstrated experimentally by Holtzman et al. (2000) for the laminar regime analysis, a pitchfork bifurcation occurs at a critical Grashof number, above which the symmetric solutions becomes unstable and finite perturbations and asymmetric solutions are instead obtained. The boundary conditions were set to match closely the conditions of the attic of houses and buildings in the wintertime (uniform temperatures T_C at the inclined walls and T_H at the base wall). The velocity components were set to zero at all boundaries. Since the velocity fluctuations are zero at the walls, the boundary conditions for k are specified at the walls, where k is set to zero. Moreover, the conditions stipulated by Jones and Launder (1972) are considered for ε, which consist of introducing the wall functions f_μ, f_1 and f_2 to the ε equation and equating ε to zero at the walls.

4. Computational procedure

The partial differential equations governing turbulent natural convection are reduced to a system of simultaneous algebraic equations by means of the control-volume based finite volume procedure. The discretization of the combined convective and diffusive fluxes across the control surfaces is modeled using the QUICK scheme of Leonard (1979), which relies on a three-point upstream-weighted quadratic interpolation for cell face values. Since the scheme is based on a quadratic function, its accuracy in terms of Taylor series truncation error is third order. Another notable feature is the fact that the discretized equations involve not only immediate-neighbor nodes but also nodes that are far away. The pressure–velocity coupling is handled with the SIMPLE scheme described by Patankar (1980). Steady-state solutions are obtained utilizing under-relaxation techniques.

Due to the coupled nature of the system equations, the under-relaxation, particularly in the energy equation, slowed the convergence rate but was necessary to generate the solutions. The under-relaxation factors of 0.3 for the pressure, 0.7 for the momentum, 0.8 for k and ε and 0.9 for the turbulent viscosity μ_T and the energy equation seem to be adequate. Based on a sequence of numerical experiments by successively increasing the grid dimensions, it was found that the mesh constructed with 75,000 quadrilateral elements as the base grid provided a good compromise between the computational efforts when contrasted with accuracy. Since the turbulent natural convection boundary layer is expected to be extremely thin, a non-uniform grid was deployed in the computational domain with nodes tightly clustered near the wall boundaries. The grid layouts chosen rendered reliable air velocity and temperature fields for the selected values of Ra_H of 1.58×10^9 and 5×10^{10}; grid independence was achieved within one percent for both values of the Rayleigh number. Local iterative convergence was assessed by monitoring the magnitude of the total heat flux across the active walls by setting its variation to less than 10^{-5}, whereas global iterative convergence was guaranteed by controlling the residuals of the conservation equations (1)–(6) by setting its variations to less than 10^{-6}.

Table 1
Comparison of the relevant flow/thermal quantities linked to an air-filled square cavity for $Ra_H = 10^6$

Quantity	Present work	De Vahl Davis (1983)
u_{max}	65.89	64.630
Y	0.87	0.850
v_{max}	221.80	217.360
X	0.04	0.038
$\overline{Nu}$	8.75	8.799

There is no comparable experimental or numerical past data for the present study on turbulent natural convection in isosceles triangular enclosures. The solution procedure has been validated for laminar natural convection employing the benchmark numerical solution of De Vahl Davis (1983) in a standard square cavity (Table 1) and the experimental results of Flack (1980) (Fig. 2) in an isosceles triangular cavity. In both cases, excellent agreements have been obtained.

Fig. 3 compares the structure of the solution obtained in the present study and the one obtained by Henkes and Hoogendoorn (1995) for $Ra = 5 \times 10^{10}$, which shows the isotherms and isolines of the turbulent viscosity. Due to

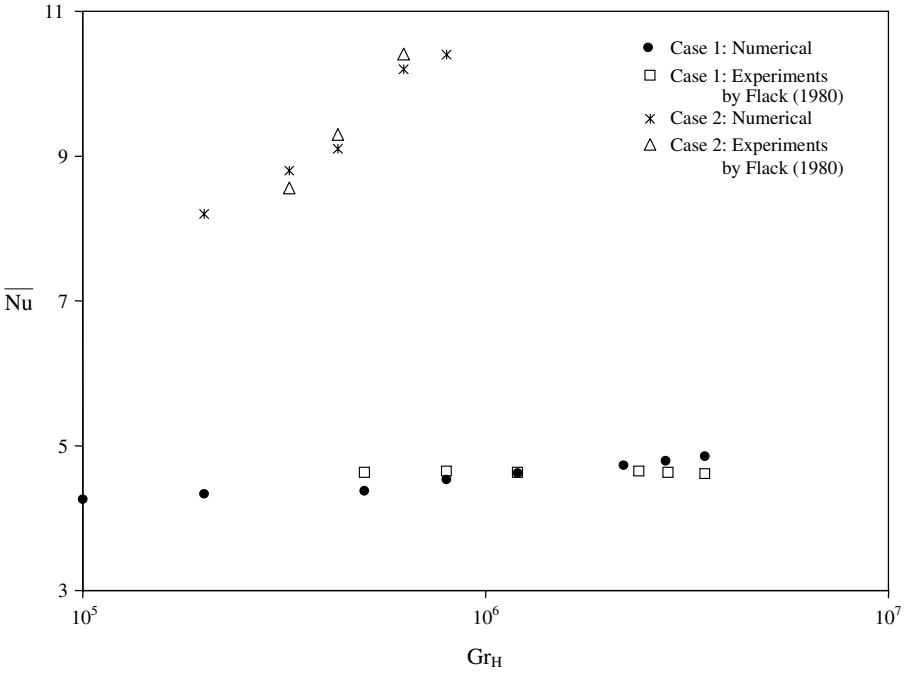

Fig. 2. Comparison between the numerical and experimental mean Nusselt numbers for summer (Cases 1) and winter (Case 2) conditions.

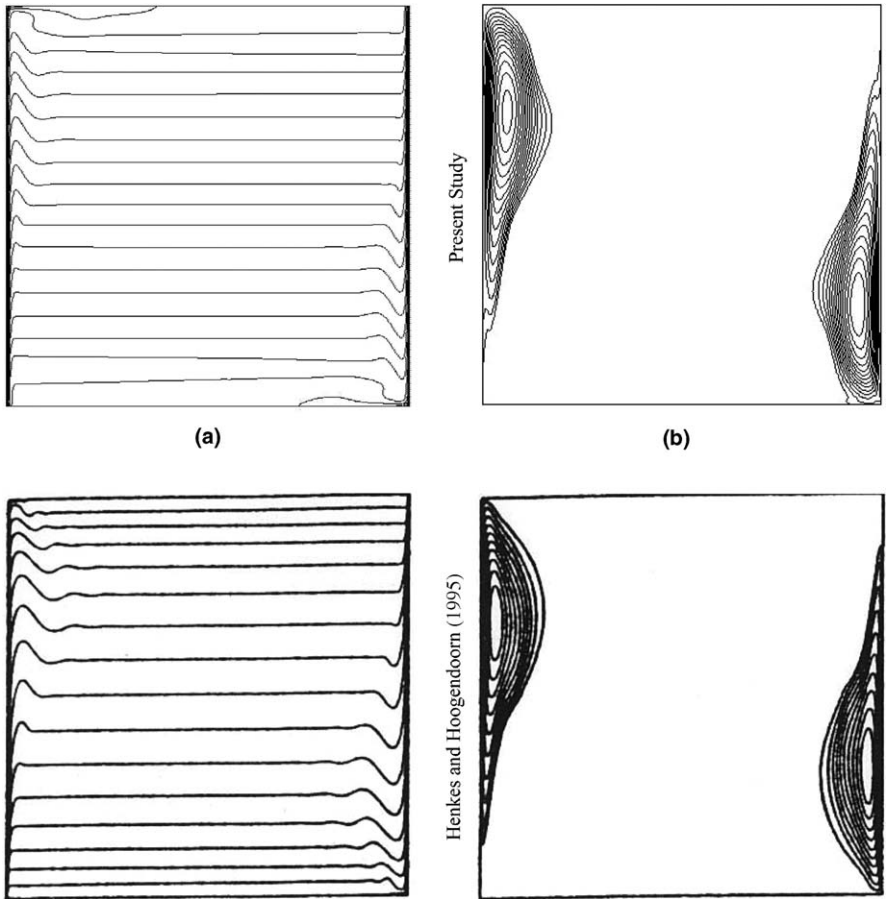

Fig. 3. Comparison of the flow structure for a square cavity at $Ra_H = 5 \times 10^{10}$ against the results of Henkes and Hoogendoorn (1995): (a) isotherms and (b) turbulent viscosity.

Table 2
Comparison of the flow patterns at $Y = 0.5$ in a square cavity against the experimental results of Ampofo and Karayiannis (2003) for $Ra_H = 1.58 \times 10^9$

X	V (m/s) Ampofo and Karayiannis (2003)	V (m/s) present work	T (°C) Ampofo and Karayiannis (2003)	T (°C) present work
0	0.0000	0.000	50.000	50.0
3.3333e−4	0.0403	0.036	48.100	47.6
1.0000e−3	0.0843	0.078	46.800	45.7
2.0000e−3	0.1325	0.125	44.740	43.8
3.0000e−3	0.1655	0.181	42.284	41.0
4.0000e−3	0.2000	0.198	40.540	38.9
0.0133	0.1745	0.187	32.620	33.0
0.0400	0.0374	0.041	30.180	29.1
0.0800	2.1470e−3	1.840e−3	31.252	30.0
0.3200	1.7200e−4	1.610e−4	31.232	30.0
0.5000	−6.9000e−5	−7.350e−5	30.696	30.0
0.6000	−1.8100e−4	−2.110e−4	30.616	30.0
0.7200	−4.9900e−4	−4.681e−4	30.808	30.0
0.8000	−2.2700e−4	−2.323e−4	30.540	30.0
0.8667	−3.1700e−4	−3.660e−4	30.316	30.0
0.9200	4.4080e−4	5.012e−4	30.244	30.0
0.9600	−0.0403	−0.046	30.792	31.3
0.9800	−0.1252	−0.142	30.188	29.2
0.9980	−0.1056	−0.110	15.296	14.5
1.0000	0.0000	0.000	10.000	10.0

the large value of the Rayleigh number, thin boundary layers have been formed along the boundaries and the turbulence is concentrated in part of the vertical boundary layer.

The vertical velocity profile at $Y = 0.5$ is compared against the experimental data of Ampofo and Karayiannis (2003) as shown in Table 2. It may be observed that the vertical

velocity increases steeply from the isothermal walls to a peak and then decreases rapidly. Meanwhile, away from the walls the fluid remains stationary. Satisfactory agreement was observed with maximum difference within 15%. Temperature profiles at the mid-plane $Y = 0.5$ is also compared with the experimental results obtained by Ampofo and Karayiannis (2003) and the comparison is presented in Table 2. A good agreement is observable with maximum differences within 4%.

5. Results and discussion

The modeled equations and the empirical relations associated with the boundary conditions were used to predict turbulent thermal convection within an isosceles triangular enclosure (Fig. 1). The upper inclined walls were maintained isothermally at T_C and the base wall was maintained isothermally at T_H ($T_H > T_C$). All results presented in this section are for $Pr = 0.71$. Two cavity dimensions of $0.86\ \text{m} \times 1.72\ \text{m}$ and $2.73\ \text{m} \times 5.46\ \text{m}$ (aspect ratio of 1/2) were considered with a temperature difference ($T_H - T_C$) of 20 K giving Rayleigh numbers of 1.58×10^9 and 5×10^{10}, respectively. Numerical results in terms of the velocity components, turbulent viscosity, turbulent kinetic energy, and temperature are presented at different locations of the enclosure along the three lines 1, 2 and 3 that identify the respective planes $X = 0.25$, 0.5 and 0.75 (see Fig. 1). Other results such as of the wall shear stresses and the local Nusselt number are plotted along the walls of the enclosure.

The structure of the solution at $Ra_H = 1.58 \times 10^9$ is given in Fig. 4, which shows the streamlines, isotherms, and isolines of the turbulent viscosity. From Fig. 4a, we observe a contour plot of the stream function where two counter-rotating vortices exist; the main vortex of high strength and large size is rotating counterclockwise and a secondary vortex of small size is located in the right corner of the enclosure. It is evident from the gradient of the stream function that the velocity is highest near the walls and thin boundary layers are formed in these regions. In contrast, the center of the geometry contains slow moving fluid as shown by the low gradient area. The isotherms indicate a large isothermal core with sharp gradients near the walls. The turbulence is concentrated in part of the boundary layers and its level is relatively high for the entire domain; the maximum turbulent viscosity is found to be 180 times the molecular viscosity. Due to the large value of the Rayleigh number, the structure of the flow is not symmetrical and justifies the choice of considering the entire physical domain for the computations. When Ra_H is increased to 5×10^{10}, in addition to the main vortex and the secondary one located in the right corner, a third vortex rotating clockwise, appears in the upper corner of the enclosure (Fig. 5a). The secondary vortex in the right corner increases in size and, together with the new one, push the main vortex to the left corner of the enclosure. The boundary layer gets thinner compared to Fig. 4a and

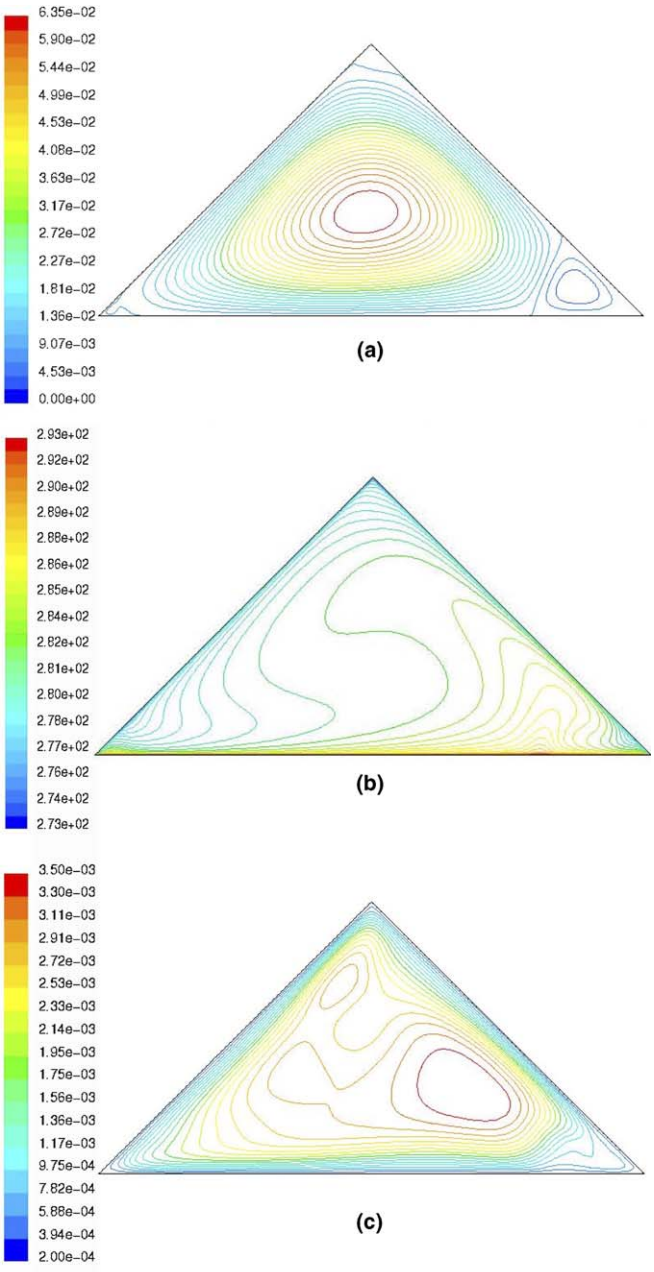

Fig. 4. Structure of the solution at $Ra_H = 1.58 \times 10^9$: (a) streamlines, (b) isotherms, and (c) turbulent viscosity.

the magnitude of the velocity gradient near the walls increases by one order of magnitude, creating higher fluid velocities. The effect of increment in Ra_H on the temperature field can be seen in the companion isotherms presented in Fig. 5b. The isoline plots of turbulent viscosity at $Ra_H = 5 \times 10^{10}$ are illustrated in Fig. 5c. When compared to Fig. 4c, the maximum turbulent viscosity increased from 180μ to 770μ. Also, the region of high viscosity moved from the right corner to the upper corner of the enclosure.

Since the geometry is symmetrical, the image of the flow structure through a vertical mirror yields also a steady-state solution of the problem. The solution images are

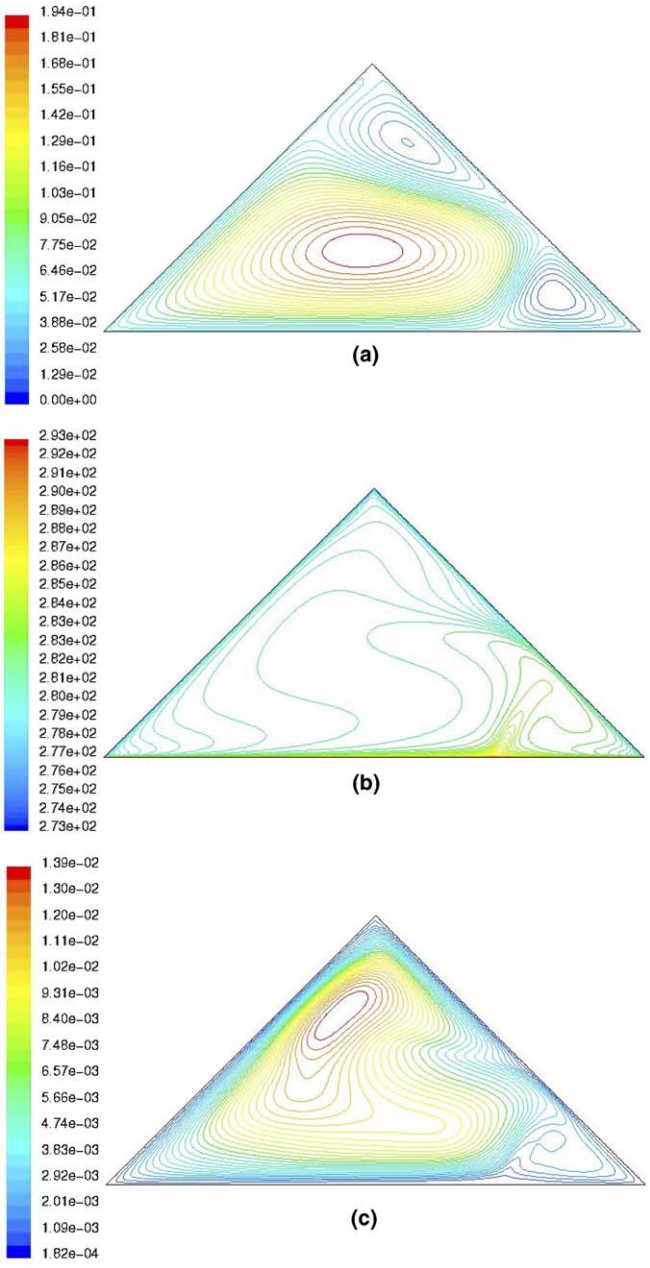

Fig. 5. Structure of the solution at $Ra_H = 5 \times 10^{10}$: (a) streamlines, (b) isotherms, and (c) turbulent viscosity.

characterized by vortices rotating in opposite directions when compared to the solutions presented in Figs. 4 and 5.

The vertical velocity profile, V, along the three lines located at $X = 0.25$, 0.5 and 0.75 is depicted in Fig. 6 for $Ra_H = 1.58 \times 10^9$. Regarding the line 1, $|V|$ increases from the hot wall to reach a maximum near the cold wall, where the fluid falls down with high velocities, and then decreases rapidly in the boundary layer to reach a zero value at the wall. At the mid-plane, V is not affected by the enclosure height; its variation remains limited. Essentially, V is characterized by the presence of two secondary maxima around $Y = 0.18$ and 0.82 followed, respectively, by a decrease towards zero between $Y = 0.45$ and 0.65 and at the right wall. At the right region where the warm fluid rises (Line 3), V increases monotonically with respect to Y to reach a maximum near the cold wall. As the enclosure ceiling is approached, the vertical velocity component decreases gradually in the boundary layer. When comparing the three curves, it can be seen that the vertical velocity is more pronounced in the left corner of the triangular geometry and minimal at the mid-plane whereas the right corner displays intermediate vertical velocities. Fig. 7 illustrates the horizontal velocity profiles at various enclosure locations. The three profiles show a steep increase in the horizontal velocity and boundary layer thickness as the fluid is warmed along the base wall. As Y increases, U decays rapidly even attaining negative values. This means that there is rotational motion or a fluid reversal at these locations. The maximum velocity in the hot wall boundary layer at the mid-plane (29 cm/s) is much higher than the corresponding value in the left (22 cm/s) and right (13 cm/s) regions of the wall, i.e., about 20% and 55% higher, respectively. This behavior is due to the sharp corners of the cavity that force the fluid to slow down before changing direction. On the other hand, the maximum velocity in the cold boundary layer along the line 1 (19 cm/s) is about 21% higher than the corresponding value in the other side along the line 3 (15 cm/s), whereas in the upper corner of the enclosure very small velocities are observed because of the enclosure shape at this corner that makes the fluid motion slow. Shown also in Fig. 7 is the difference in the U profile along the mid-plane when compared against the two other profiles; it has a minimum at $Y = 0.7$ far from the boundary layer and presents a second flow reversal in the upper corner. The zero value of U at $Y = 0.93$ is a characteristic of the limit between the two counter-rotating vortices. Compared to the square enclosure, the horizontal velocity component has the same order of magnitude as the vertical velocity. However, it was demonstrated experimentally by Tian and Karayiannis (2000a) that the horizontal velocity component is one order of magnitude smaller than the vertical component, and its distribution changes significantly at different heights.

The turbulent viscosity, μ_T, along the three planes located at $X = 0.25$, 0.5 and 0.75 is provided in Fig. 8 for $Ra_H = 1.58 \times 10^9$. Its magnitude is minimal at the base wall and 13 times higher than the molecular viscosity μ. The value of μ_T at the wall was found to be independent of X and stays constant along the wall. As Y increases, a high gradient of μ_T is observed in the boundary layer which results in increased turbulence in these regions. The monotonic increasing behavior of μ_T with respect to Y continues to reach a maximum and stays at high values until the effect of the upper wall on the fluid becomes important; it then diminishes smoothly towards the second minimum at the upper wall. This minimum value is a little higher than the corresponding value at the base wall (about 16μ). Regarding the maximum values of μ_T: line 3 presents the highest, which is 178 times the molecular viscosity, and line 1 presents the lowest at about 135μ; the mid-plane (line 2)

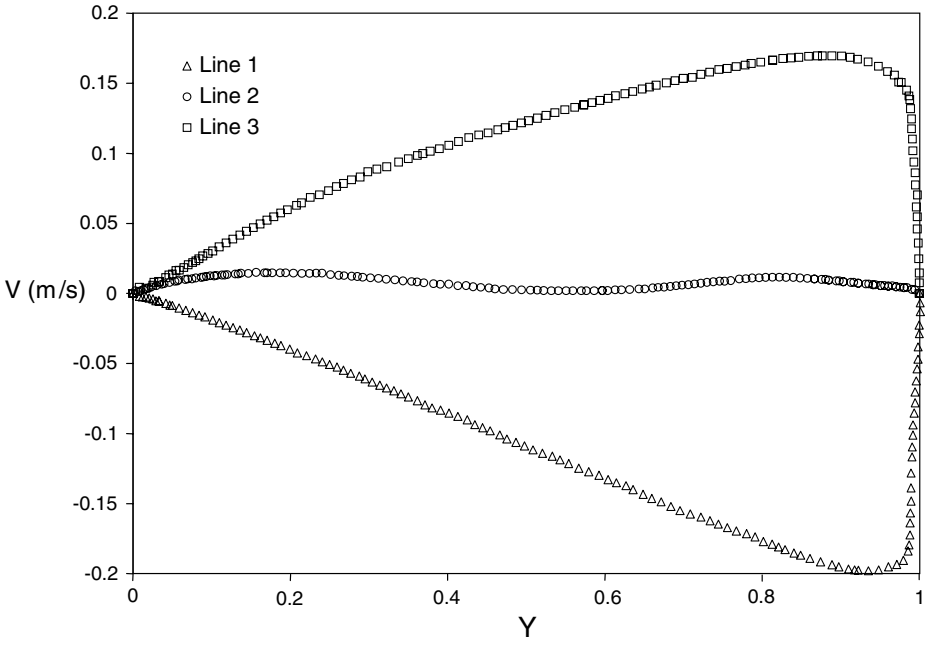

Fig. 6. Vertical velocity profiles along the three lines located at $X = 0.25$, 0.5 and 0.75 for $Ra_H = 1.58 \times 10^9$.

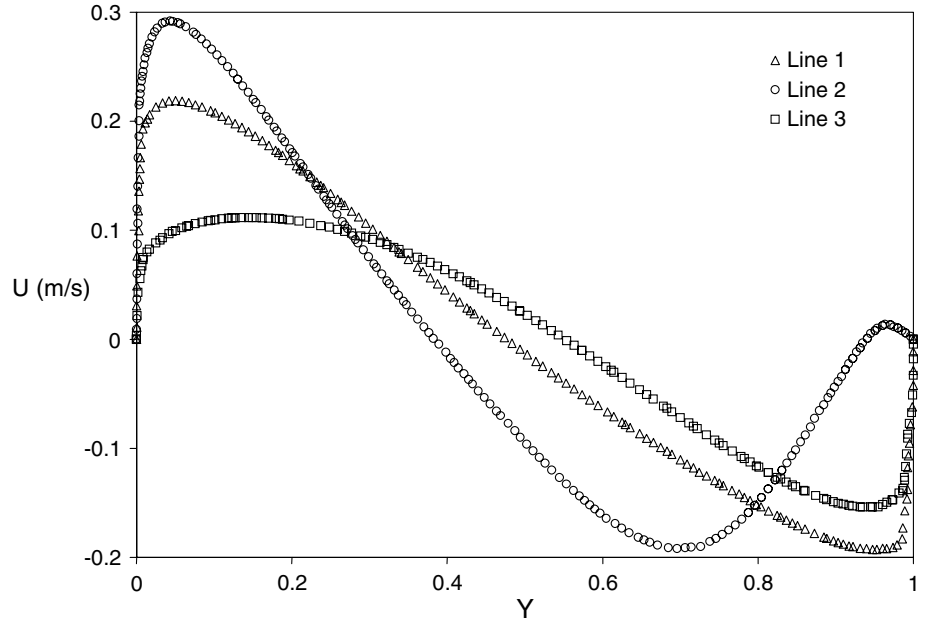

Fig. 7. Horizontal velocity profiles along the three lines located at $X = 0.25$, 0.5 and 0.75 for $Ra_H = 1.58 \times 10^9$.

displays an intermediate value of about 162μ. This result is confirmed by the contours of isolines of μ_T (Fig. 4), which show high turbulent viscosity in the right region of the enclosure where the stream of hot fluid is directed upward. Again the triangular geometry was found to bring forward high turbulence levels when compared to the square cavity, where the maximum of μ_T is about 60 times the molecular viscosity μ for a Prandtl number of 0.71 (Heindel et al., 1994) even though their Rayleigh number was higher. The same authors found that this value increases as the Pr number decreases. The same results were obtained earlier by Henkes et al. (1991) and Lage and Bejan (1991).

The turbulent kinetic energy, k, along the three typical planes of the triangular enclosure at $Ra_H = 1.58 \times 10^9$ increases in the viscous layer, reaches a maximum, and drops smoothly when approaching the upper wall (see Fig. 9). One feature observed in the figure is the difference between the k-curve at the mid-plane and the two other k-curves. The former exhibits two maximums at $Y = 0.14$ and $Y = 0.83$ and a minimum in the core region of the

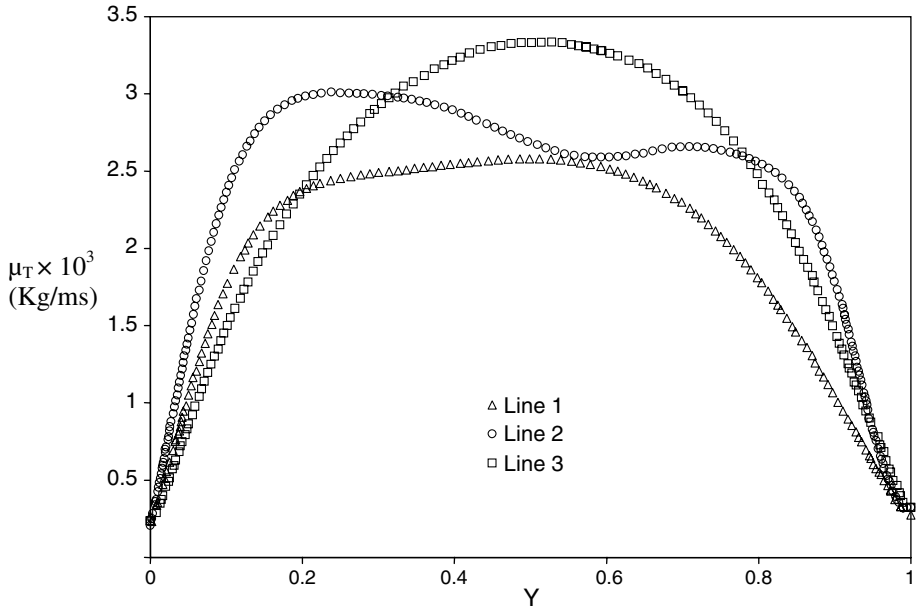

Fig. 8. Turbulent viscosity distribution along the three lines located at $X = 0.25$, 0.5 and 0.75 for $Ra_H = 1.58 \times 10^9$.

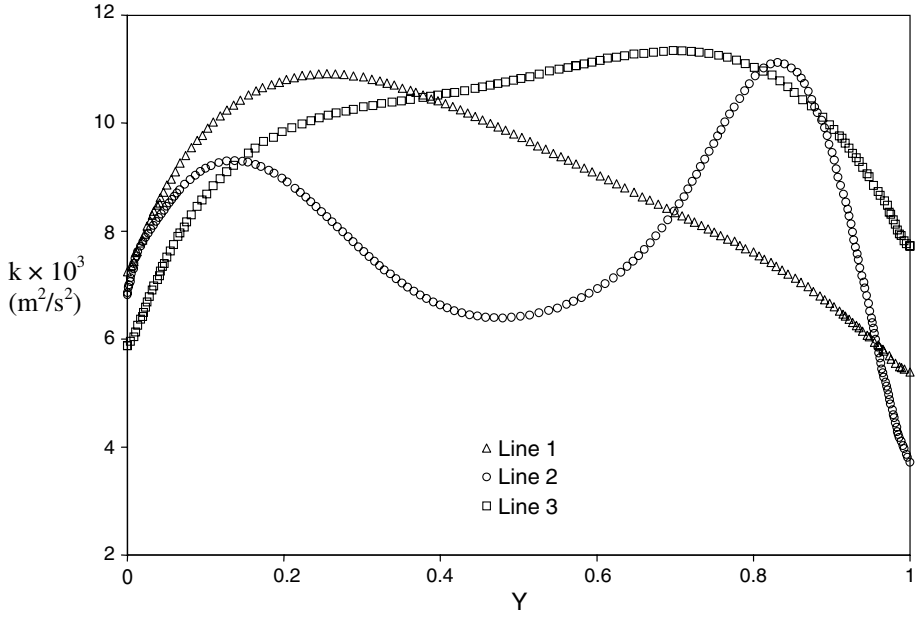

Fig. 9. Turbulent kinetic energy along the three lines located at $X = 0.25$, 0.5 and 0.75 for $Ra_H = 1.58 \times 10^9$.

enclosure where the flow motion is slow and the magnitude of the velocity fluctuations is small. Fig. 9 also shows that the turbulent kinetic energy is higher near the base wall in the left region of the enclosure and when approaching the upper wall in the right region. The qualitative shape of the k distribution along the mid-plane is similar to the corresponding distribution along the mid-plane $Y = H/2$ of a square cavity. This patterns clearly indicates that the turbulent flow is limited to the boundary layer and its intensity increases along the flow direction as observed by Tian and Karayiannis (2000a,b).

As mentioned above, the two upper walls were kept at 0 °C while the base wall was kept at 20 °C. A typical temperature distribution at different places of the enclosure is depicted in Fig. 10 at $Ra_H = 1.58 \times 10^9$. The temperature of the core was 9.8 °C which is nearly equal to the mean temperature. Across the cavity in the vertical direction, the temperature changes rapidly near the isothermal walls in a very narrow strip ($\Delta Y = 0.06$ from the wall). From $Y = 0.1$ to 0.9 along the lines 1 and 3 and from $Y = 0.1$ to 0.78 along the line 2, the temperature changed only slightly indicating that the fluid in the core area was nearly

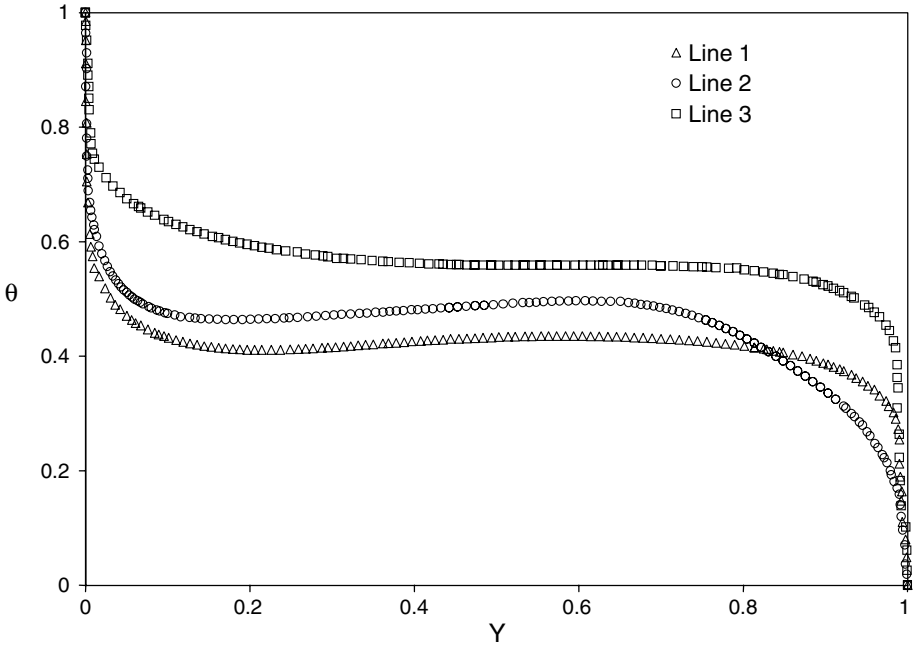

Fig. 10. Temperature distribution along the three lines located at $X = 0.25$, 0.5 and 0.75 for $Ra_H = 1.58 \times 10^9$.

isothermal. Along the line 2, the temperature starts to decrease sharply far from the upper wall around $Y = 0.8$; this tendency is due to the low fluid velocities in the region and the inclined cold walls, which keep the upper corner of the enclosure cold. In the sub-interval between $Y = 0$ and 0.8, the temperature is higher along the line 3 and lower along the line 1; this is the result of the counterclockwise movement of the main vortex that forces the hot fluid to rise in the right region and the cold fluid to fall in the left region.

In this section we are interested in examining how the turbulent boundary layer behaves near the walls and how it carries heat away from or into the walls. The velocity profile at Ra_H of 1.58×10^9 in the viscous layer is used to determine the wall shear stress, τ_w, along different walls of the enclosure and the results are presented in Fig. 11. At the corners, the velocity is zero so the wall shear stress is zero. Then, with the formation of the boundary layer, the peak velocity increases along the fluid direction so that the velocity gradient in the viscous layer increases. At $X = 0.02$ (along the base wall), $Z_1 = 0.07$ (along the left inclined wall), and $Z_2 = 0.18$ (along the right inclined wall) the wall shear stress reaches its first maximum, corresponding to the first peak. This peak is the result of the flow circulation in the corners of the triangle. After those points, the wall shear stress diminishes smoothly to collapse to a zero value at the intersection between the two counter-rotating vortices (the secondary vortices in the corner and the main vortex). The magnitude of the peaks is proportional to the strength of the secondary vortex. Far from the corners τ_w raises again to reach the maximum where high velocities exist. This maximum occurs at $X = 0.43$ for the base wall and around $Z_1 = Z_2 = 0.52$ along the inclined walls. When approaching the corners, τ_w decreases sharply to form another peak caused by the small anti-clockwise vortices. We now compare the τ_w curves for the triangular enclosure against the experimental data of Ampofo and Karayiannis (2003) and Tian and Karayiannis (2000a) along the active walls of a square enclosure (results are not presented); their results show only one peak for each wall. Also, the magnitude of the peak is around 1.7×10^{-3} Pa for both active walls which is about 50% and 27% less than the corresponding values at the base and inclined walls, respectively.

The local and average Nusselt numbers on the hot and cold walls can be determined using the calculated temperatures in the thermal boundary layer (Patankar, 1980). The end product is

$$Nu = -\frac{H^2}{L(T_H - T_C)} \left.\frac{\partial T}{\partial n}\right|_{wall} \quad \text{for the inclined walls} \tag{11a}$$

$$Nu = -\frac{H^2}{W(T_H - T_C)} \left.\frac{\partial T}{\partial n}\right|_{wall} \quad \text{for the base wall} \tag{11b}$$

Here, n is the normal direction to the wall. From this definition, the heat transfer from the hot wall into the cavity and from the cavity into the cold walls is positive. The local Nusselt number on the hot and cold walls of the cavity is shown in Fig. 12. Nu begins with a large value at the point where the discontinuities $X = 0$ and $X = 1$ occur. The Nu value is about 200 for the base wall and 135 for both inclined walls. The heat transfer at these points occurs only by conduction and justifies the way the two inclined walls and the base wall share the same values at $X = 0$ and $X = 1$. Away from these points, the heat conduction still dominates the process of heat transfer and Nu decreases as the distance between the hot and cold walls increases.

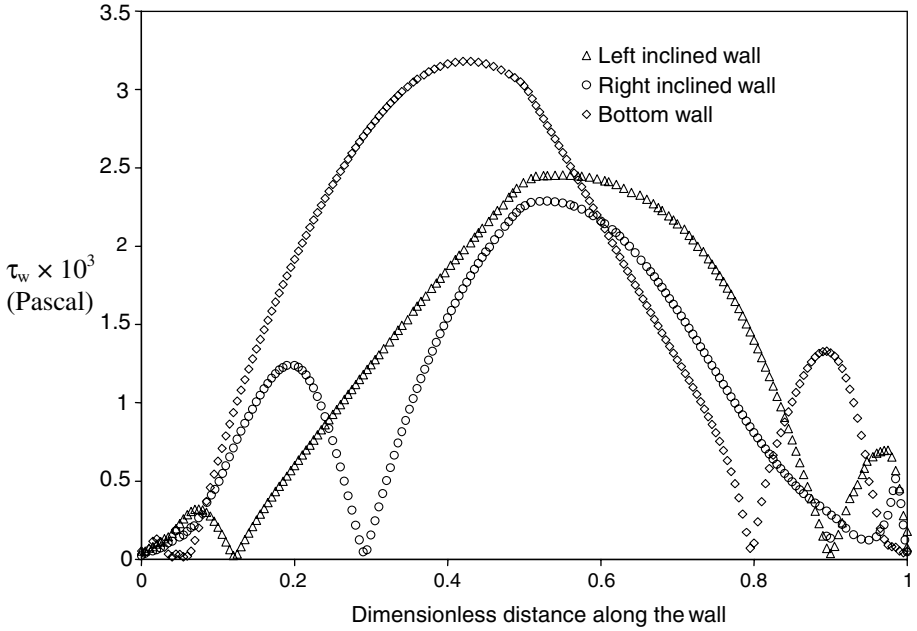

Fig. 11. Wall shear stress along the isothermal walls at $Ra_H = 1.58 \times 10^9$.

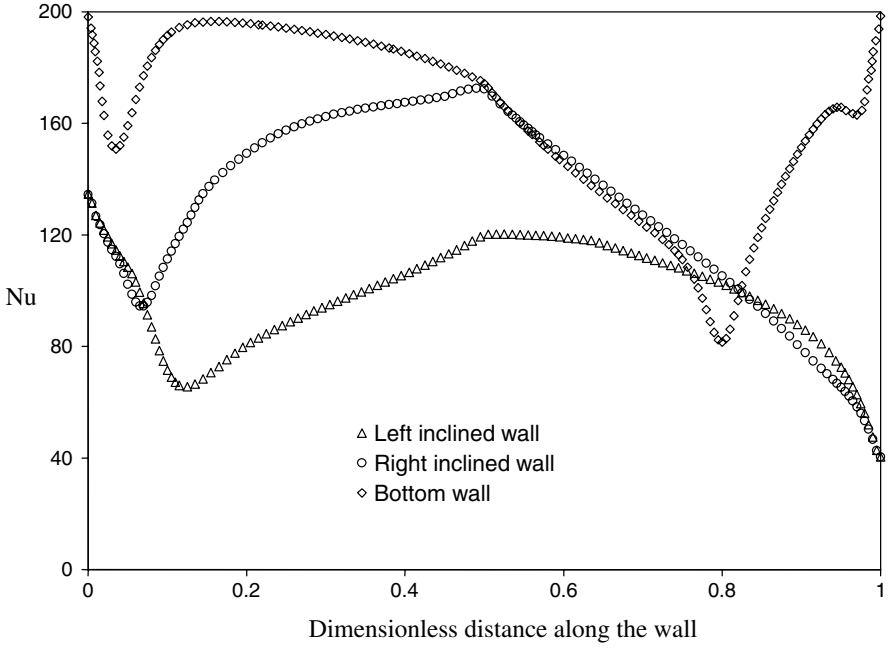

Fig. 12. Local Nusselt number profiles along the isothermal walls at $Ra_H = 1.58 \times 10^9$.

This tendency continues and Nu reaches a minimum at $X = 0.03$ for the base wall, $Z_2 = 0.06$ for the right inclined wall, and $Z_1 = 0.11$ for the left inclined wall. This minimum heat transport corresponds to the onset of convection as the fluid velocity increases along the walls. As the velocity increases, the thermal boundary layer gets thinner and Nu grows to a maximum and then drops smoothly as the thickness of the boundary layer increases. This behavior prevails for the inclined walls and Nu is minimal at the upper corner of the enclosure. However, for the base wall, Nu passes through a minimum around $X = 0.8$ and grows quickly when approaching the $X = 1$ discontinuity, indicating the important contribution of heat transfer by conduction in this region. The minimum Nu at $X = 0.8$ corresponds to the region where the hot stream is diverted from the wall and the thermal boundary layer is not as thin as in the other regions of the wall.

In synthesis, the magnitude of the average Nusselt number, $\overline{Nu}$, turns out to be 163.14, 131.82, and 99.58 for the base, right and left inclined walls, respectively. The huge

difference for the two inclined walls is accounted for by the direction of the main vortex, in which the hot fluid rises along the right cold wall and falls in a cooled stream on the left wall.

6. Conclusions

A numerical investigation of two-dimensional turbulent natural convection in an air-filled isosceles triangular cavity was conducted for two values of Rayleigh number; 1.58×10^9 and 5×10^{10}. Under these conditions, the fluid flow in the cavity was turbulent. The fluid flows in a narrow strip along the walls where the velocity and temperature change sharply. In the horizontal boundary layer, the velocity reaches its maximum value between the buoyant sub-layer and the outer layer and decreases to a minimum value at the outer edge of the boundary. The negative values of V on the left and U in the upper regions are the results of rotational motion of the two vortices. The fluid in the cavity core stays stationary and stratified. The wall shear stress was obtained from the velocity component in the viscous layer. Qualitatively, similar distributions were obtained for the three walls which are characterized by three peaks, one on each corner much smaller in magnitude than the main peak that takes place in high velocity region of the walls. It is important to point out that, the turbulent quantities μ_T and k are reported for the first time in an isosceles triangular geometry. For a fixed Rayleigh number, this geometry holds high turbulence levels when compared to the square cavity. The maximum turbulent viscosity μ_T is found to be 770 times the molecular viscosity μ whereas this value is only about 60 for the square cavity (Heindel et al., 1994) at high Rayleigh number of 5×10^{10}. The heat transfer is large at the lower corners of the enclosure and takes place by conduction. However, away from the corners, the natural convection dominates the process of heat transfer. For instance, the average Nusselt number associated to the right inclined wall is found to be 25% higher than the corresponding value connected to the left inclined wall.

References

Akinsete, V.A., Coleman, T.A., 1982. Heat transfer by steady laminar free convection in triangular enclosures. Int. J. Heat Mass Transfer 25, 991–998.

Ampofo, F., Karayiannis, T.G., 2003. Experimental benchmark data for turbulent natural convection in an air filled square cavity. Int. J. Heat Mass Transfer 46, 3551–3572.

Asan, H., Namli, L., 2000. Laminar natural convection in a pitched roof of triangular cross section: summer day boundary condition. Energy and Buildings 33, 69–73.

Bradshaw, P., Cebeci, T., Whitelaw, J.H., 1981. Engineering Calculation Methods for Turbulent Flow. Academic Press, London.

Champagne, F.H., Pao, Y.H., Wygnanski, I.J., 1976. On the two-dimensional mixing region. J. Fluid Mech. 74, 209–250.

Del Campo, E.M., Sen, M., Ramos, E., 1988. Analysis of laminar convection in a triangular enclosure. Numer. Heat Transfer 13, 353–372.

De Vahl Davis, G., 1983. Natural convection of air in a square cavity: a benchmark numerical study. Int. J. Numer. Meth. Fluids 3, 227–248.

Flack, R.D., 1979. Velocity measurements in two natural convection air flows using a laser velocimeter. J. Heat Transfer 101, 256–260.

Flack, R.D., 1980. The experimental measurement of natural convection heat transfer in triangular enclosures heated or cooled from below. J. Heat Transfer 102, 770–772.

Gutmark, E., Wygnanski, I., 1976. The planar turbulent jet. J. Fluid Mech. 73, 465–495.

Haese, P.M., Teubner, M.D., 2002. Heat exchange in an attic space. Int. J. Heat Mass Transfer 45, 4925–4936.

Heindel, T.J., Ramadhyani, S., Incropera, F.P., 1994. Assessment of turbulence models for natural convection in an enclosure. Numer. Heat Transfer Part B 26, 147–172.

Henkes, R.A.W.M., Hoogendoorn, C.J., 1995. Comparison exercise for computations of turbulent natural convection in enclosures. Numer. Heat Transfer, Part B 28, 59–78.

Henkes, R.A.W.M., Van Der Vlugt, F.F., Hoogendoorn, C.J., 1991. Natural convection flow in a square cavity calculated with low-Reynolds-number turbulence models. Int. J. Heat Mass Transfer 34, 377–388.

Holtzman, G.A., Hill, R.W., Ball, K.S., 2000. Laminar natural convection in isosceles triangular enclosures heated from below and symmetrically cooled from above. J. Heat Transfer 122, 485–491.

Iyican, L., Bayazitoglu, Y., Witte, L.C., 1980a. An analytical study of natural convective heat transfer within a trapezoidal enclosure. J. Heat Transfer 102, 640–647.

Iyican, L., Bayazitoglu, Y., Witte, L.C., 1980b. An experimental study of natural convection in a trapezoidal enclosure. J. Heat Transfer 102, 648–653.

Jones, W.P., Launder, B.E., 1972. The prediction of laminarization with a 2-equation model of turbulence. Int. J. Heat Mass Transfer 15, 301–314.

Lage, J.L., Bejan, A., 1991. The *Ra–Pr* domain of laminar natural convection in an enclosure heated from the side. Numer. Heat Transfer, Part A 19, 21–41.

Lam, C.K.G., Bremhorst, K.A., 1981. Modified Form of the k–ε model for predicting wall turbulence. J. Fluids Eng. 103, 456–460.

Lam, S.W., Gani, R., Symons, J.G., 1989. Experimental and numerical studies of natural convection in trapezoidal cavities. J. Heat Transfer 111, 372–377.

Lee, T.S., 1991. Numerical experiments with fluid convection in tilted nonrectangular enclosures. Numer. Heat Transfer, Part A 19, 487–488.

Leonard, B.P., 1979. A stable and accurate convective modeling procedure based on quadratic upstream interpolation. Comput. Meth. Appl. Mech. Eng. 19, 59–98.

Moukalled, F., Acharya, S., 1997. Buoyancy-induced heat transfer in partially divided trapezoidal cavities. Numer. Heat Transfer, Part A 32, 787–810.

Moukalled, F., Acharya, S., 2000. Natural convection in trapezoidal cavities with baffles mounted on the upper inclined surfaces. Numer. Heat Transfer, Part A 37, 545–565.

Patankar, S.V., 1980. Numerical Heat Transfer and Fluid Flow, Hemisphere. Taylor & Francis Group, New York.

Peric, M., 1993. Natural convection in trapezoidal cavities. Numer. Heat Transfer, Part B 24, 213–219.

Poulikakos, D., Bejan, A., 1983. The fluid mechanics of an attic space. J. Fluid Mechanics 131, 251–269.

Ridouane, E.H., Campo, A., 2005. Experimental-based correlations for the characterization of free convection of air inside isosceles triangular cavities with variable apex angles. Experimental Heat Transfer 18, 81–86.

Ridouane, E. H., Campo, A. Hasnaoui, M., in press. Benefits derivable from connecting the bottom and top walls of attic enclosures with insulated vertical walls. Numer. Heat Transfer.

Salmun, H., 1995. Convection patterns in a triangular domain. Int. J. Heat Mass Transfer 38, 351–362.

Tian, Y.S., Karayiannis, T.G., 2000a. Low turbulence natural convection in an air filled square cavity. Part I: The thermal and fluid flow fields. Int. J. Heat Mass Transfer 43, 849–866.

Tian, Y.S., Karayiannis, T.G., 2000b. Low turbulence natural convection in an air filled square cavity. Part II: The turbulent quantities. Int. J. Heat Mass Transfer 43, 867–884.

Versteeg, H.K., Malalasekera, W., 1995. An Introduction to Computational Fluid Dynamics: The Finite Volume Method. Prentice Hall, Essex, UK.

Wygnanski, I., Champagne, F., Marasli, B., 1986. On the large-scale structure in two-dimensional, small-deficit, turbulent wakes. J. Fluid Mech. 168, 31–71.